First Measurement of the Q2 Dependence of the Beam-Normal Single Spin Asymmetry for Elastic Scattering off Carbon

Esser, A.; Thiel, M.; Achenbach, P.; Aulenbacher, K.; Baunack, S.; Beričič, J.; Bosnar, Damir; Correa, L.; Dehn, M; Distler, M. O.; ...

First Measurement of the Q^2 Dependence of the Beam-Normal Single Spin Asymmetry for Elastic Scattering off Carbon

A. Esser,[1] M. Thiel,[1,*] P. Achenbach,[1] K. Aulenbacher,[1] S. Baunack,[1] J. Beričič,[2] D. Bosnar,[3] L. Correa,[4] M. Dehn,[1] M. O. Distler,[1] H. Fonvieille,[4] I. Friščić,[3,†] M. Gorchtein,[1] S. Heidrich,[1] P. Herrmann,[1] M. Hoek,[1] S. Kegel,[1] Y. Kohl,[1] T. Kolar,[5,2] H.-J. Kreidel,[1] F. E. Maas,[1] H. Merkel,[1] M. Mihovilovič,[1,2] J. Müller,[1] U. Müller,[1] F. Nillius,[1] C. Palatchi,[6] K. D. Paschke,[6] J. Pochodzalla,[1] B. S. Schlimme,[1] M. Schoth,[1] F. Schulz,[1] S. Širca,[5,2] B. Spruck,[1] S. Štajner,[2] V. Tioukine,[1] A. Tyukin,[1] A. Weber,[1] and C. Sfienti[1]

[1]*Institut für Kernphysik, Johannes Gutenberg-Universität Mainz, D-55099 Mainz, Germany*
[2]*Jožef Stefan Institute, SI-1000 Ljubljana, Slovenia*
[3]*Department of Physics, Faculty of Science, University of Zagreb, 10000 Zagreb, Croatia*
[4]*Clermont Université, Université Blaise Pascal, CNRS/IN2P3, LPC, BP 10448, F-63000 Clermont-Ferrand, France*
[5]*Department of Physics, University of Ljubljana, SI-1000 Ljubljana, Slovenia*
[6]*University of Virginia, Charlottesville, Virginia 22903, USA*

(Received 13 March 2018; revised manuscript received 27 May 2018; published 11 July 2018)

We report on the first Q^2-dependent measurement of the beam-normal single spin asymmetry A_n in the elastic scattering of 570 MeV vertically polarized electrons off ^{12}C. We cover the Q^2 range between 0.02 and 0.05 GeV$^2/c^2$ and determine A_n at four different Q^2 values. The experimental results are compared to a theoretical calculation that relates A_n to the imaginary part of the two-photon exchange amplitude. The result emphasizes that the Q^2 behavior of A_n given by the ratio of the Compton to charge form factors cannot be treated independently of the target nucleus.

DOI: 10.1103/PhysRevLett.121.022503

Over the last 60 years, electron scattering experiments with ever increasing precision offer manifold opportunities to study the structure of nuclei. The technological progress nowadays allows us to perform parity-violating electron scattering experiments [1] with statistical and systematic errors better than 1 ppb. Such experiments at the precision frontier enable measurements of the strangeness contribution to the vector form factors of the proton [2–4], the weak charge of the proton and the weak mixing angle θ_W [5–7], and the neutron-skin thickness of heavy nuclei [8]. Moreover, driven by recent theoretical predictions, new experiments are planned to determine parity-violating asymmetries as a portal to physics beyond the standard model (Ref. [9], and references therein). Two boson exchange corrections play a major role in interpreting many experiments at the precision frontier but represent a considerable difficulty theoretically. Such is the case with the γZ box in parity-violating electron scattering [10], the γW box in nuclear β decays [11], and the 2γ box in form-factor measurements [12]. Dispersion relations have established themselves as the main tool for such calculations. The imaginary part of the two boson exchange diagram serves as input in these calculations, so a direct measurement of this imaginary part provides a valuable test of theoretical calculations. Experimentally, the imaginary (absorptive) part of the two-photon exchange amplitude can be accessed through the beam-normal single spin asymmetry (or the so-called transverse asymmetry) A_n in elastic scattering of electrons polarized perpendicular to the scattering plane off unpolarized nucleons. The transverse asymmetry arises from the interference of the one-photon and two-photon exchange amplitudes [13] and is defined as

$$A_n = \frac{\sigma_\uparrow - \sigma_\downarrow}{\sigma_\uparrow + \sigma_\downarrow}, \tag{1}$$

where $\sigma_\uparrow$ ($\sigma_\downarrow$) represents the cross section for the elastic scattering of electrons with spin vector $\vec{P}_e$ parallel (antiparallel) to the normal vector, defined by $\hat{n} = (\vec{k} \times \vec{k}')/|\vec{k} \times \vec{k}'|$. $\vec{k}$ and $\vec{k}'$ are the three-momenta of the incident and scattered electrons, respectively. The experimentally measured asymmetry A_{exp} is related to A_n by

$$A_{\mathrm{exp}} = A_n \vec{P}_e \cdot \hat{n}. \tag{2}$$

The calculations for the theoretical treatment of two-photon exchange processes in general kinematics are challenging because they require an account of inclusive hadronic intermediate states with arbitrary virtualities of the exchanged photons. By considering only the very low momentum transfer region ($m_e c \ll Q \ll E/c$), where the leading order is $\sim C_0 \log(Q^2/m_e^2 c^2)$, this complication is alleviated [14,15]. Since the coefficient C_0 is obtained in a model-independent way from the optical theorem as an energy-weighted integral over the total photoabsorption

cross section on the particular target, this expression can be calculated exactly.

Calculations of A_n for the reaction $p(\vec{e}, e')p$ using this inclusive approach [14,15], as well as models with a partial account of the excited hadronic spectrum [16,17], provide a good description of forward scattering data [18] and a reasonably good description of large scattering angle data [19–22], with the exception of the backward scattering data of Ref. [23]. Gorchtein and Horowitz [24] generalized the forward inclusive model to nuclear targets:

$$A_n \sim C_0 \log\left(\frac{Q^2}{m_e^2 c^2}\right) \frac{F_{\mathrm{Compton}}(Q^2)}{F_{\mathrm{ch}}(Q^2)}. \tag{3}$$

For the Compton slope parameter, only data for the proton and for ^{4}He are available, suggesting that the relevant Q^2 behavior for A_n given by the ratio of the Compton to charge form factors

$$\frac{F_{\mathrm{Compton}}(Q^2)}{F_{\mathrm{ch}}(Q^2)} \approx \exp\left[-4Q^2/(\mathrm{GeV}^2/c^2)\right] \tag{4}$$

is roughly independent of the target. The calculation was compared to forward scattering data ($\theta \leq 6°$) taken at the Jefferson Laboratory on ^{1}H ($Q^2 \approx 0.10\ \mathrm{GeV}^2/c^2$), ^{4}He ($Q^2 \approx 0.08\ \mathrm{GeV}^2/c^2$), ^{12}C, and ^{208}Pb ($Q^2 \approx 0.01\ \mathrm{GeV}^2/c^2$) [18]: while the calculation is in good agreement with the observed asymmetries for lighter targets, it fails completely to reproduce the ^{208}Pb data. This has a major impact on parity-violating electron scattering experiments since the transverse asymmetry, arising from a nonzero vertical component of the beam polarization, produces false asymmetries that contribute substantially to the total systematic error. This contribution will become even more crucial for future experiments [9,25] aiming at a precision much higher than ever attained before. Systematic studies of A_n dependencies on the momentum transfer, the nuclear charge, and the energy are absolutely mandatory to benchmark the current theoretical description of A_n, thus also providing new insight into the structure of nuclei. The aim of our measurement is to perform the first systematic study of the Q^2 dependence of the beam-normal single spin asymmetry for light nuclei.

The experiment was performed at the spectrometer setup of the A1 Collaboration at the Mainz Microtron MAMI [26]. The polarized 570 MeV electrons were produced using a strained GaAs/GaAsP super lattice photocathode that was irradiated with circularly polarized laser light [27,28]. The longitudinal spin of the electrons leaving the photocathode was rotated to transverse orientation (in the horizontal plane) using a Wien filter which was positioned between the 100 keV polarized electron source and the injector linac of the accelerator. The polarization vector was finally rotated to vertical orientation using a pair of solenoids, located shortly behind the Wien filter. The orientation of the electron beam polarization vector was alternating between up and down by setting the high voltage of a fast Pockels cell in the optical system of the polarized electron source. The orientation as well as the degree of polarization were determined and monitored during the whole measuring campaign [29]. This was accomplished using a Mott polarimeter [30] downstream of the 3.5 MeV injector linac and a Møller polarimeter [31] close to the interaction point in the spectrometer hall. The degree of vertical polarization was deduced by subtracting the horizontal polarization components from the total polarization and was, on average, $P_e = 82.7\% \pm 0.3\%(\mathrm{stat}) \pm 1.1\%(\mathrm{syst})$.

For the measurement of the beam-normal single spin asymmetry A_n, a 20 μA continuous-wave beam of vertically polarized electrons was impinging on a 2.27 g/cm^2 carbon target. Elastically scattered electrons were focused onto two fused-silica detectors positioned in the focal plane of the two high-resolution spectrometers A and B of the A1 setup [32], located to the left and right sides of the incoming beam, respectively. The fused-silica detectors were oriented at 45° with respect to the direction of the electrons in the spectrometer. The sizes of the two fused-silica bars [$(300 \times 70 \times 10)\ \mathrm{mm}^3$ and $(100 \times 70 \times 10)\ \mathrm{mm}^3$] were chosen according to the different focal plane geometries of the two spectrometers. The produced Cherenkov light was detected by 25 mm fused-silica–window photomultipliers directly attached to the fused-silica bars: five for the detector in spectrometer A and three for the detector in spectrometer B.

To reach a sufficiently high count rate, the detectors had to be placed in the most forward direction. Limited by the distance between the exit beam line and its quadrupole, spectrometer A was placed at its minimum angle of 23.50°, which corresponds to $Q^2 = 0.04\ \mathrm{GeV}^2/c^2$, at a beam energy of 570 MeV. In accordance with its smaller focal plane, spectrometer B was placed at 20.61° to cover the same momentum range. This measurement allowed for identification of possible false asymmetries due to helicity-correlated changes of the beam parameters. With this configuration, the extracted asymmetries for each spectrometer were equal within the experimental uncertainties (see Fig. 3), thus confirming a negligible contribution to beam-related false asymmetries. Therefore, three more Q^2 measurements were performed during the same experiment by changing the kinematical configuration of the spectrometers: one measurement at $Q^2 = 0.05\ \mathrm{GeV}^2/c^2$ by placing spectrometer A at 25.90°, and two more measurements at $Q^2 = 0.03\ \mathrm{GeV}^2/c^2$ and $Q^2 = 0.02\ \mathrm{GeV}^2/c^2$ made by placing spectrometer B at 17.65° and 15.11°, respectively.

During the experiment, the fused-silica detectors were operated in two different modes. The position of the Cherenkov detectors within the elastic line was optimized during the low current mode ($I = 50$ nA). For this purpose the fused-silica detectors were read out in coincidence with

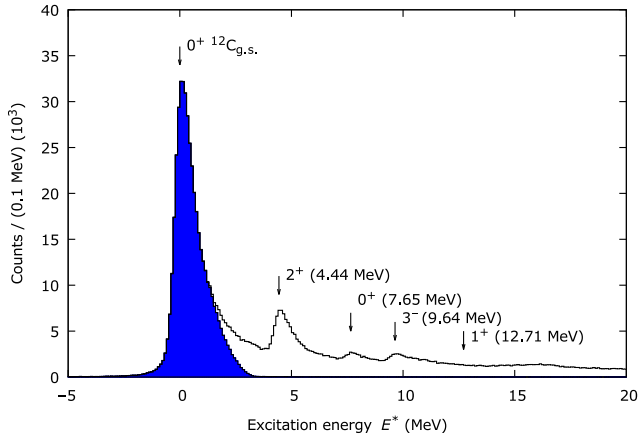

FIG. 1. The excitation energy spectrum shows the acceptance of the spectrometer without Cherenkov cut (black line) and of the Cherenkov detector only (shaded area). By changing the magnetic field of the spectrometer, the elastic peak was moved until it matched the position of the Cherenkov detector.

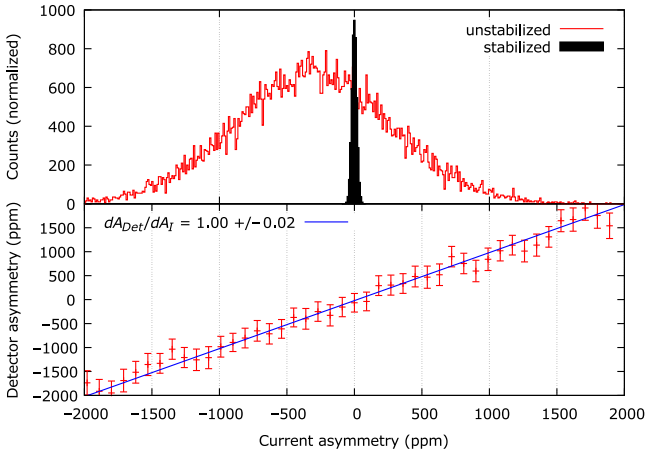

FIG. 2. (Top panel) Comparison between the asymmetry in the integrated signal from a beam-current monitor observed in a run with beam stabilization off (red) and with beam stabilization on (black). (Bottom panel) Raw asymmetry determined for one PMT of the Cherenkov detector in spectrometer B as a function of the current asymmetry for a run without beam stabilization.

the vertical drift chambers of the spectrometers. The obtained excitation energy spectrum shown in Fig. 1 demonstrates the clear separation between elastic and inelastic events from the first excited state of carbon at 4.4 MeV.

In the high current (or integrating) mode, the amplification of the photomultiplier tubes (PMTs) was reduced from nominal to avoid a nonlinear behavior. While all other detector components of the spectrometers were switched off to prevent additional noise, the fused-silica detectors were read out with parts of the former A4 experiment data acquisition system [2]. The response of each PMT was recorded with an analog-to-digital converter, integrating the charge over periods of 20 ms. A gate generator provided the integration windows where the polarization is reversed in patterns like $\uparrow\downarrow\downarrow\uparrow$ or $\downarrow\uparrow\uparrow\downarrow$ in a pseudorandom sequence. Moreover, an additional $\lambda/2$-wave plate was periodically inserted into the laser system of the source to identify possible false asymmetries and to suppress many systematic effects.

In order to minimize helicity-correlated beam fluctuations, four dedicated stabilization systems [beam current, beam energy, slow position (dc), and fast position (ac)] were used at MAMI. The beam parameters were measured by several monitors, placed in the A1 beam line, which were read out together with the detector signals. As an example, Fig. 2 (top panel) shows the impact of the beam-current stabilization system on the current asymmetry.

Moreover, calibration runs over the full beam-current range as well as in a narrow region around 20 μA were performed regularly to monitor the functioning and the linearity of the PMTs.

We calculate the raw detector asymmetry A_{raw} as

$$A_{\text{raw}} = \frac{N_e^{\uparrow} - N_e^{\downarrow}}{N_e^{\uparrow} + N_e^{\downarrow}}, \tag{5}$$

where $N_e^{\uparrow(\downarrow)}$ denotes the integrated detector signal which is proportional to the detected number of elastically scattered electrons for each polarization state. Even though with our dedicated stabilization systems helicity-correlated changes of the beam parameters were suppressed as well as possible, tiny remnants can always lead to false asymmetries. Therefore, correction factors $c_i (i = 1, \ldots, 6)$ were applied to the beam-current asymmetry A_I, the horizontal and vertical beam position differences Δx and Δy, the horizontal and vertical beam angle differences $\Delta x'$ and $\Delta y'$, and the beam energy difference ΔE to determine the experimental asymmetry

$$A_{\text{exp}} = A_{\text{raw}} - c_1 A_I - c_2 \Delta x - c_3 \Delta y - c_4 \Delta x' - c_5 \Delta y' - c_6 \Delta E. \tag{6}$$

Typically, the correction factors would be derived from a multidimensional regression of the measured asymmetry versus the corresponding parameters. However, because of the extraordinarily high-quality beam during the experimental campaign, the variation of the parameters was too narrow compared to the width of the asymmetry to apply this method. Instead, analytical calculations as well as simulations were used to determine the individual correction factors. The factor c_1 in Eq. (6) must be equal to 1 since the luminosity changes linearly with the beam current. This correlation has been verified in runs taken without the beam-current stabilization system, as illustrated in Fig. 2 (bottom panel). The factors c_2 and c_3 for position-related false asymmetries were estimated by using Monte Carlo simulations. In addition, a small data sample acquired without beam stabilizations was used as a cross-check, and both results were in good agreement. Concerning the beam

TABLE I. Measured beam-normal single spin asymmetries for each spectrometer and kinematical setting, with the corresponding statistical and systematic uncertainty contributions in ppm.

Spectrometer	B	B	B	A	A
Setup	3	2	1	1	2 and 3
Q^2 (GeV$^2/c^2$)	0.023	0.030	0.041	0.039	0.049
A_n	−15.984	−20.672	−21.933	−23.877	−28.296
Energy fluctuation δE	0.007	0.006	0.009	0.009	0.001
Current asymmetry δI	0.013	0.015	0.011	0.011	0.010
Vertical beam position δy	0.003	0.001	0.005	0.005	0.002
Horizontal beam position δx	0.001	0.003	0.005	0.023	0.012
Vertical angle $\delta y'$	0	0	0	0	0
Horizontal angle $\delta x'$	0.003	0.001	0.001	0.001	0.001
Gate length	0.013	0.010	0.010	0.010	0.008
P_e measurement	0.245	0.385	0.480	0.523	0.491
PMT gain variation	0.380	0.130	1.100	0.170	0.030
Total systematic error	0.664	0.551	1.621	0.752	0.555
Statistical error	1.061	0.959	1.515	0.967	1.372

angle differences, an analytical derivation of a parametrization of the Mott cross section was used to determine the correction factor c_4 for the horizontal scattering angle. The correction factor c_5 for the vertical scattering angle vanishes since the angular acceptance of both spectrometers is symmetric with respect to their bending planes. Nevertheless, variations of the vertical scattering angle will cause changes of the effective degree of polarization by up to 1%. This effect could be corrected by using the position information from the vertical drift chambers obtained during the low current mode. Since the sign of the energy fluctuation variation is unknown, no corrections could be applied in this case. Therefore, it has been treated as a contribution to the systematic error. Besides the beam-related systematic uncertainties, the major contribution to the total systematic error comes from the aging of the PMTs, which results in a reduction of gain, especially when running at high count rates. The relationship between a given PMT's gain reduction and its corresponding nonlinearity was studied with frequently performed calibration runs, postexperiment. Retroactive corrections (0.064 ppm $< c_{\mathrm{PMT}} < 0.588$ ppm) were applied to the data based on gain degradation. The larger corrections for the setups $B1$ and $B3$ are due to malfunctioning voltage dividers and the high count rate, respectively. Furthermore, current unstabilized runs were taken intermittently during the run period. These runs were used to estimate the dA/dI deviation from unity (Fig. 2, bottom panel) and to characterize the degree of nonlinearity which had developed in each PMT. The individual contributions to the total systematic uncertainty are summarized in Table I.

To confirm the feasibility of the experimental method and the analysis procedure as well, the experimental asymmetry A_{exp} was first extracted for setup 1 (see Table I), where both spectrometers covered the same momentum range. Figure 3 shows the measured A_{exp} in each spectrometer and for each PMT. The asymmetries obtained with both detector systems were, as expected, similar in magnitude but of opposite sign since $\hat{n}$ in Eq. (2) reverses sign. In addition, it can be seen that the sign of the asymmetry also consistently changed when the additional $\lambda/2$-wave plate was moved into the laser beam of the polarized electron source.

Finally, the experimental asymmetry A_{exp} was normalized to the electron beam polarization to extract the physics asymmetry A_n. The experimentally determined values for all four kinematic configurations, and the corresponding statistical and systematic uncertainties are summarized in Table I. For illustration, the data are shown in Fig. 4.

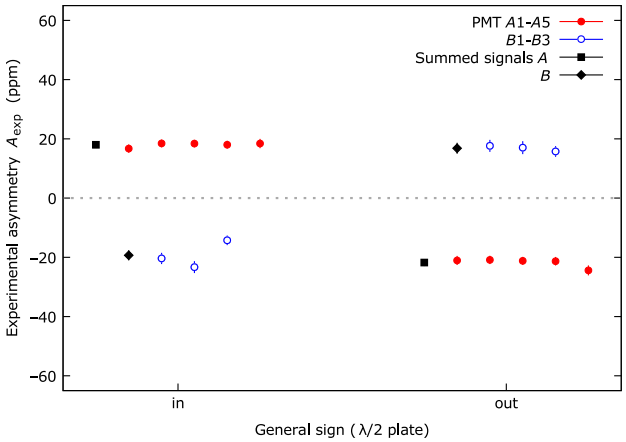

FIG. 3. The transverse asymmetry A_{exp} for each PMT of the detectors placed in spectrometer A (filled red circles) and spectrometer B (open blue circles) at $Q^2 = 0.04$ GeV$^2/c^2$. By inserting an additional $\lambda/2$-wave plate into the laser beam of the polarized electron source, the general sign changed.

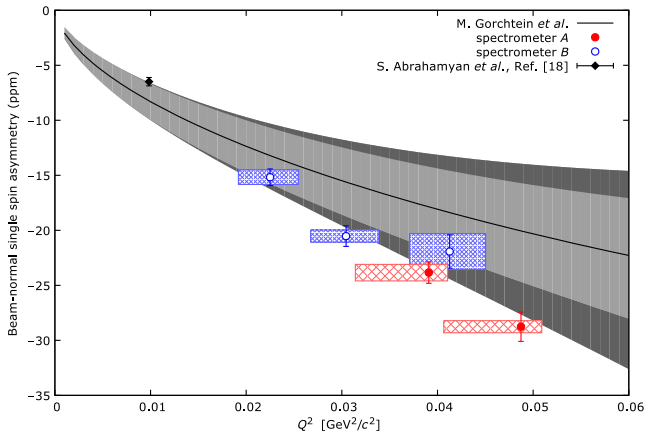

FIG. 4. Extracted transverse asymmetries A_n for the detectors placed in spectrometer A (filled red circles) and spectrometer B (open blue circles) versus Q^2. The width of the given boxes indicates the full width at half maximum of the Q^2 distribution, which is determined by the intersection of the angular acceptance of the spectrometers and the geometry of the detectors. The statistical and systematic uncertainties are given by the error bars and the height of the boxes, respectively. The theoretical calculation for $E_b = 0.570$ GeV of Ref. [24] (black line) is shown for comparison. The given bands belong to the uncertainty of the Compton slope parameter of 10% (light grey) and 20% (dark grey). In addition, the result of the PREX Collaboration (black diamond) at $E_b = 1.063$ GeV [18] is shown.

The curve represents the leading Q^2 behavior, as calculated in the model of Ref. [24] upon neglecting corrections $\sim Q^2/E^2$. The given uncertainty of the theoretical prediction is obtained from two sources: the Compton slope parameter for the ^{12}C target and terms not enhanced by the large logarithm (see Ref. [24] for details). The two are expected to be independent and are added in quadrature. The Compton slope parameter introduced in Eq. (4) was allowed to vary within 10% and 20% of the central value, corresponding to the inner and outer bands shown in Fig. 4. The comparison of the data with the model indicates that the assumption of the dominance of the $\log(Q^2/m_e^2c^2)$ term and the independence of $F_{\mathrm{Compton}}(Q^2)/F_{\mathrm{ch}}(Q^2)$ of the target nucleus in Eq. (4), successfully describing ^{1}H and ^{4}He data, reproduces the ^{12}C data only within a 20% uncertainty. Even larger deviations could be expected for heavier nuclei.

Future measurements at MAMI will investigate the transverse asymmetry for heavier nuclei at the same Q^2 values. This will serve, together with the current data set, as an important input for future theoretical calculations to achieve better control of the two-photon exchange mechanism, and they might contribute to a deeper understanding of the structure of nuclei.

We acknowledge the MAMI accelerator group and all the workshop staff members for the outstanding support. We thank Krishna Kumar for the many stimulating discussions and valuable suggestions in the preparation of the experiment. This work was supported by the PRISMA (Precision Physics, Fundamental Interactions and Structure of Matter) Cluster of Excellence, the Deutsche Forschungsgemeinschaft through the Collaborative Research Center 1044 and the Federal State of Rhineland-Palatinate.

*thielm@uni-mainz.de
†Present address: MIT-LNS, Cambridge, MA 02139, USA.

[1] D. H. Beck and R. D. McKeown, Parity violating electron scattering and nucleon structure, Annu. Rev. Nucl. Part. Sci. **51**, 189 (2001).
[2] F. E. Maas *et al.* (A4 Collaboration), Measurement of Strange-Quark Contributions to the Nucleon's Form Factors at $Q^2 = 0.230(\mathrm{GeV}/c)^2$, Phys. Rev. Lett. **93**, 022002 (2004).
[3] D. S. Armstrong *et al.* (G0 Collaboration), Strange-Quark Contributions to Parity-Violating Asymmetries in the Forward G0 Electron-Proton Scattering Experiment, Phys. Rev. Lett. **95**, 092001 (2005).
[4] K. A. Aniol *et al.* (HAPPEX Collaboration), Constraints on the nucleon strange form-factors at $Q^2 \sim 0.1$ GeV^2, Phys. Lett. B **635**, 275 (2006).
[5] P. L. Anthony *et al.* (SLAC E158 Collaboration), Precision Measurement of the Weak Mixing Angle in Møller Scattering, Phys. Rev. Lett. **95**, 081601 (2005).
[6] D. Androic *et al.* (Qweak Collaboration), First Determination of the Weak Charge of the Proton, Phys. Rev. Lett. **111**, 141803 (2013).
[7] D. Androic *et al.* (Qweak Collaboration), Precision measurement of the weak charge of the proton, Nature (London) **557**, 207 (2018).
[8] S. Abrahamyan *et al.*, Measurement of the Neutron Radius of ^{208}Pb Through Parity-Violation in Electron Scattering, Phys. Rev. Lett. **108**, 112502 (2012).
[9] D. Becker *et al.*, The P2 Experiment–A future high-precision measurement of the electroweak mixing angle at low momentum transfer, arXiv:1802.04759.
[10] M. Gorchtein, C. J. Horowitz, and M. J. Ramsey-Musolf, Model-dependence of the γZ dispersion correction to the parity-violating asymmetry in elastic ep scattering, Phys. Rev. C **84**, 015502 (2011).
[11] W. J. Marciano and A. Sirlin, Improved Calculation of Electroweak Radiative Corrections and the Value of V_{ud}, Phys. Rev. Lett. **96**, 032002 (2006).
[12] A. Afanasev, P. G. Blunden, D. Hasell, and B. A. Raue, Two-photon exchange in elastic electron-proton scattering, Prog. Part. Nucl. Phys. **95**, 245 (2017).
[13] A. De Rujula, J. M. Kaplan, and E. De Rafael, Elastic scattering of electrons from polarized protons and inelastic electron scattering experiments, Nucl. Phys. **B35**, 365 (1971).
[14] A. V. Afanasev and N. P. Merenkov, Collinear photon exchange in the beam normal polarization asymmetry of elastic electron-proton scattering, Phys. Lett. B **599**, 48 (2004).

[15] M. Gorchtein, Doubly virtual Compton scattering and the beam normal spin asymmetry, Phys. Rev. C **73**, 035213 (2006).
[16] B. Pasquini and M. Vanderhaeghen, Single spin asymmetries in elastic electron-nucleon scattering, Eur. Phys. J. A **24**, 29 (2005).
[17] B. Pasquini and M. Vanderhaeghen, Resonance estimates for single spin asymmetries in elastic electron-nucleon scattering, Phys. Rev. C **70**, 045206 (2004).
[18] S. Abrahamyan *et al.* (HAPPEX and PREX Collaborations), New Measurements of the Transverse Beam Asymmetry for Elastic Electron Scattering from Selected Nuclei, Phys. Rev. Lett. **109**, 192501 (2012).
[19] F. E. Maas *et al.*, Measurement of the Transverse Beam Spin Asymmetry in Elastic Electron Proton Scattering and the Inelastic Contribution to the Imaginary Part of the Two-Photon Exchange Amplitude, Phys. Rev. Lett. **94**, 082001 (2005).
[20] D. S. Armstrong *et al.* (G0 Collaboration), Transverse Beam Spin Asymmetries in Forward-Angle Elastic Electron-Proton Scattering, Phys. Rev. Lett. **99**, 092301 (2007).
[21] D. Androic *et al.* (G0 Collaboration), Transverse Beam Spin Asymmetries at Backward Angles in Elastic Electron-Proton and Quasi-elastic Electron-Deuteron Scattering, Phys. Rev. Lett. **107**, 022501 (2011).
[22] D. Balaguer Ríos *et al.*, New Measurements of the Beam Normal Spin Asymmetries at Large Backward Angles with Hydrogen and Deuterium Targets, Phys. Rev. Lett. **119**, 012501 (2017).
[23] S. P. Wells *et al.* (SAMPLE Collaboration), Measurement of the vector analyzing power in elastic electron proton scattering as a probe of double photon exchange amplitudes, Phys. Rev. C **63**, 064001 (2001).
[24] M. Gorchtein and C. J. Horowitz, Analyzing power in elastic scattering of the electrons off a spin-0 target, Phys. Rev. C **77**, 044606 (2008).
[25] J. Benesch *et al.* (MOLLER Collaboration), The MOLLER Experiment: An Ultra-Precise Measurement of the Weak Mixing Angle Using Møller Scattering, arXiv:1411.4088.
[26] H. Herminghaus, A. Feder, K. H. Kaiser, W. Manz, and H. Von Der Schmitt, The design of a cascaded 800-MeV normal conducting CW racetrack microtron, Nucl. Instrum. Methods **138**, 1 (1976).
[27] K. Aulenbacher *et al.*, The MAMI source of polarized electrons, Nucl. Instrum. Methods Phys. Res., Sect. A **391**, 498 (1997).
[28] K. Aulenbacher, Polarized beams for electron accelerators, Eur. Phys. J. Spec. Top. **198**, 361 (2011).
[29] B. S. Schlimme *et al.*, Vertical beam polarization at MAMI, Nucl. Instrum. Methods Phys. Res., Sect. A **850**, 54 (2017).
[30] K. H. Steffens, H. G. Andresen, J. Blume-Werry, F. Klein, K. Aulenbacher, and E. Reichert, A Spin rotator for producing a longitudinally polarized electron beam with MAMI, Nucl. Instrum. Methods Phys. Res., Sect. A **325**, 378 (1993).
[31] A. Tyukin, Entwicklung, Vorbereitung und Durchführung eines Experiments zur Paritätsverletzung an der A1 Spektrometer Anlage, Master's thesis, Johannes Gutenberg-Universität Mainz, 2015.
[32] K. I. Blomqvist *et al.*, The three-spectrometer facility at the Mainz microtron MAMI, Nucl. Instrum. Methods Phys. Res., Sect. A **403**, 263 (1998).